RESEARCH ARTICLE

The removal of tetracycline, oxytetracycline, and chlortetracycline by manganese oxide–doped copper oxide: the behaviors and insights of Cu-Mn combination for enhancing antibiotics removal

Kun Wu[1,2] · Chuanqiao Zhang[1] · Ting Liu[3] · Hang Lei[3] · Shengjiong Yang[1] · Pengkang Jin[1]

Abstract

Adsorption process is suitable to the advanced treatment of tetracycline antibiotics (TCs; including tetracycline (TTC), oxytetracycline (OTC), and chlortetracycline (CTC)) in poultry wastewater. In this research, Mn oxide-doped Cu oxide (MODCO) was synthesized and used for the removal of TTC, OTC, and CTC. According to the XRD and SEM analysis results, MODCO has an amorphous crystal structure and is formed by the aggregation of nano-sized particles with a uniform distribution of Cu and Mn elements. In addition, MODCO has a BET surface area of 67.7 m^2/g and a pH$_{IEP}$ value of 7.8. The results of batch experiments illustrated that the reaction rates for the removal of three TCs were in the order of OTC > CTC > TTC. In addition, the theoretical maximum amounts of TTC, OTC, and CTC adsorbed on MODCO were determined to be 2.90 mmol/g, 4.15 mmol/g, and 2.20 mmol/g via the Langmuir model, respectively. The optimal removal performances of TCs were achieved in the pH range of 6~9, and the coexistence of anions posed an unnoticeable effect on the removal efficiencies. The spectroscopic analysis results demonstrated that the removal mechanism of TCs was mainly attributed to surface complexation. Furthermore, a part of TCs may be decomposed by Mn oxides during the removal process according to the UV spectrogram results. Overall, MODCO has exhibited a great potential for the removal of TCs from aqueous solution.

Keywords Tetracycline antibiotics · Adsorption · Oxidation · Mn oxides · Cu oxides

Introduction

Tetracycline antibiotics (TCs), which mainly include tetracycline (TTC), oxytetracycline (OTC), and chlortetracycline (CTC) and have broad-spectrum antibacterial properties, are one of the most widely used antibiotics in the world (Liu et al. 2018a). These antibiotics have been extensively used not only in the medical industry but also as veterinary drugs, growth promoters, and preservatives in aquaculture (Yan et al. 2013).

Although tetracycline antibiotics bring huge economic benefits, the environmental pollution problems caused by the abuse of them cannot be ignored. Previous studies reported that only a small part of antibiotics consumed by animals or human are absorbed in their bodies, and up to 95% of consumed antibiotics enter surface water, groundwater, and soil in the form of maternal or metabolites, such as feces, urine, and other excreta (Grujić et al. 2009; Zhou et al. 2013). In addition, hospital sewage and pharmaceutical wastewater may also contain large amounts of antibiotic substances (Watkinson et al. 2009). Watkinson et al. (2009) reported that about 80% of total antibiotics were removed from wastewater in wastewater treatment plants (WWTPs), but at the same time, only 30% of TCs were reduced. When such wastewater is discharged into water bodies, it will pose a great threat to the ecological safety of the water environment. Wang et al. 2019a pointed out that

✉ Kun Wu
tomlikeit@gmail.com

1 School of Environmental and Municipal Engineering, Xi'an University of Architecture and Technology, No.13, Yanta Road, Beiling District, Xi'an 710055, Shaanxi, China

2 Key Laboratory of Water Resource, Environment and Ecology, MOE, Xi'an 710055, China

3 College of Resources and Environment, Northwest A&F University, Yangling 712100, Shaanxi, China

tetracycline antibiotics were detected in most of the major water bodies in China and other countries. For example, TTC, OTC, and CTC were detected in the Tiaoxi River of China with the maximum concentrations of 623.43; 19,809.81; and 47.52 ng/L, respectively (Li et al. 2016). Additionally, the maximum concentrations of TTC, OTC, and CTC detected in the Han River and the Kyungahn Stream of South Korea reached 2093, 1236, and 793 ng/L, respectively (Kim et al. 2016). Excessive tetracycline antibiotics in the environment can cause great harm to human health. Previous studies have shown that the residual tetracycline antibiotics can enter the human body through the food chain, leading to adverse reactions such as human poisoning, and even serious cancerous changes (Kushikawa et al. 2016; Liu et al. 2018a). In addition to these dominant hazards, it is more alarming that a large amount of tetracycline may lead to the production of resistant microorganisms and resistance genes, and thus increasing the resistance of human body and even producing super resistant bacteria (Liu et al. 2019). Hence, it is widely recognized that the pollution problem of tetracycline antibiotics in water environment cannot be ignored.

The search for efficient and practical methods of tetracycline removal has become a research focus of water treatment technologies. Extensive researches have been conducted on the removal of antibiotics from water. The methods for TC removal mainly include biological and physicochemical treatment technologies. However, due to the lack of experience in design and operation, most of the biological methods are still in the experimental stage for the treatment of TC wastewater (Liu et al. 2018b; Xu et al. 2019). On the other hand, the current commonly physicochemical methods for treating TC wastewater include coagulation (Saitoh et al. 2014), photocatalytic oxidation (Wang et al. 2019b), ozone oxidation (Li et al. 2008), and adsorption (Bangari and Sinha 2019). Although, coagulation technology has the advantages of effective treatment performance, simple equipments, easy maintenance operation, and adjustable operating time. Unfortunately, the coagulation technology is restricted due to the problem of chemical sludge management (Homem and Santos 2011). Ozone technology is regarded as an alternative method due to its fast reaction rate and strong oxidation activity, but the electricity high consumption for producing ozone and the potentially toxic by-products have hampered its engineering applications (Li et al. 2008). Photocatalytic oxidation processes have the virtues of fast reaction speed, low cost, and no secondary pollution, but most of them are still in the theoretical research and laboratory stage due to the problems of narrow application range, poor catalyst reusability, difficult reactor design, and high energy consumption (Belhouchet et al. 2019; Gao et al. 2018). Compared with the above methods, adsorption technology is a better choice for removing TCs because of its simplicity, ease of operation, high efficiency, relatively low cost, and no high toxicity by-products (Bangari and Sinha

2019). The adsorbents that have been used to adsorb TC wastewater include zeolite (de Sousa et al. 2018), activated carbon (Selmi et al. 2018), clays (Premarathna et al. 2019), and metal oxides (Liu et al. 2012). In the past decade, the development of novel metal adsorbents has gradually become a new research hotspot because of their remarkable adsorption performance for the removal of many organic or inorganic substances (Liu et al. 2012; Ma et al. 2019). Metal oxides commonly used in the current removal of antibiotics include iron oxides (Cao et al. 2018), aluminum oxides (Gu and Karthikeyan 2005), manganese oxides (Rubert 2006), and composite metal oxides (Xu et al. 2009). Liu et al. (2012) synthesized Fe-Mn binary oxide by a simultaneous oxidation and co-precipitation process to remove tetracycline, which exhibited a satisfactory performance. Hydrous manganese oxides are the strongest natural oxidants found in soils. Rubert (2006) used hydrous manganese oxide to remove oxytetracycline, and they found that oxytetracycline could be degraded via MnO_2 oxidation. Ma et al. (2019) prepared Fe/Cu composite-loaded active municipal waste sludge biochar for the removal of tetracycline from water. It was found that Cu had great ability to chelate or complex with -COOH and -OH. It can be anticipated that a Cu-Mn binary oxide has the potential to oxidize and adsorb tetracycline simultaneously. Moreover, many studies have reported excellent performance of the removal of inorganic contaminants by Cu or Mn oxides and their derivatives due to their strong ability of adsorption or oxidation, respectively (Liu et al. 2015; Zhang et al. 2013). However, to our best knowledge, the removal performances and mechanisms of TCs by using Cu-Mn binary oxide have never been reported in the existing literature. In this study, the removal characteristics of TCs onto a newly synthesized Cu-Mn binary oxide (MODCO) were investigated. Furthermore, SEM-EDS, FTIR, and XPS were conducted to investigate the removal mechanism of TCs on MODCO.

Materials and methods

Materials

Chemicals in this work, including copper(II) nitrate trihydrate ($Cu(NO_3)_2 \cdot 3H_2O$), manganese(II) chloride tetrahydrate ($MnCl_2 \cdot 4H_2O$), potassium permanganate ($KMnO_4$), and sodium hydroxide (NaOH), were of analytical grade and used without further purification. All solutions were prepared by deionized water. All reaction glass vessels employed in experiments were soaked and cleaned with 1% nitric acid (HNO_3) and rinsed several times with deionized water before use. Sodium hydroxide (NaOH) and nitric acid (HNO_3) solutions were employed to adjust the pH of solution. The partial characteristics of three antibiotics are listed in Table S1.

The preparation of MODCO

Via the preliminary evaluation of the synthetic method, MODCO was synthesized by a two-step method including precipitation and oxidation, and Cu/Mn = 3:1 was chosen as the optimal molar ratio for adsorbent preparation. The synthesizing procedure was as follows: (1) First, a certain amount of $Cu(NO_3)_2 \cdot 3H_2O$ was dissolved in deionized water. Under vigorous stirring, 0.1 M of NaOH solution was added into $Cu(NO_3)_2$ solution to maintain the pH of mixed solution around 8.0. The suspension was continuously stirred for 10 min, aged at ambient temperature for several hours, and washed several times with deionized water, filtrated and dried at 60 °C for 12 h. The dried material was crushed and stored in desiccator for the next step. (2) After that, a certain amount of $MnCl_2 \cdot 4H_2O$ was dissolved in deionized water, then the material obtained in the former step was added into $MnCl_2$ solution under vigorous stirring, and certain volume of 0.1 M of $KMnO_4$ was slowly added into the mixture. Afterwards, 0.1 M of NaOH solution was added into the mixed solution to maintain the pH between 5.0 and 6.0. The subsequent steps of filtration, drying, and grinding are the same as the previous step. The finally obtained material named MODCO was stored in a desiccator for use.

Batch experiments

To evaluate the maximum removal capacity of MODCO, batch experiments were carried out at 25 ± 1 °C with initial TC concentration varied from 0.02 to 1.40 mmol/L. A series of 150-mL conical flasks were loaded with 50 mL of solution containing TTC (or OTC or CTC) and added with 15.0 mg of MODCO. The pH of suspensions was adjusted to 7.0 ± 0.1 by adding 0.1 M of NaOH and HNO_3 during the experiment. After shaking at 180 rpm for 24 h, the samples were collected and filtered with a 0.45-μm membrane filter and analyzed for TTC/OTC/CTC concentration. To evaluate reaction kinetics, initial TC concentrations were set as 0.1 mmol/L and 0.5 mmol/L, respectively. In each test, 15 mg of sorbents were added into 150-mL conical flasks containing 50 mL of TTC/OTC/CTC solution to obtain a 0.3 g/L suspension. These flasks were shaken in an orbit shaker, and the suspension pH was maintained at 7.0 ± 0.1. After the samples were collected at predetermined time intervals and filtered with a 0.45-μm membrane, the residual concentration of TTC/OTC/CTC in the filtrates was analyzed. To assess the influence of solution pH on TC removal by MODCO, batch experiments were conducted by adding 15 mg of MODCO to 150-mL conical flasks containing 50 mL of solution with initial TTC/OTC/CTC concentration of 0.1 mmol/L or 0.5 mmol/L at 25 ± 1 °C. The pH of solutions was adjusted with NaOH and HNO_3 solutions to specified values in the range of 3~10 during the experiments. After shaking the conical flasks on an orbit shaker at 180 rpm

for 24 h, all samples were collected, filtered through a 0.45-μm membrane, and analyzed. To study the effect of commonly coexisting ions in water, such as sulfate, silicate, carbonate, phosphate, and calcium ion, as well as magnesium ion, on the removal of TCs, batch tests were carried out by adding ion-corresponding salt to 50 mL of 0.5-mmol/L TTC/OTC/CTC solution to obtain an coexisting ion concentration ranged from 2 to 10 mmol/L. A total of 15 mg of MODCO was added into each test to obtain a 0.3-g/L suspension. Each test was shaking at 180 rpm for 24 h at 25 ± 1 °C, and the solution pH was maintained at 7.0 ± 0.1 by using 0.1 M of NaOH and HNO_3 during the removal process. After filtration by a 0.45-μm polycarbonate filter membrane, the concentration of residual TTC/OTC/CTC solution was analyzed using UV spectrophotometer.

Analytical and characterization methods

The concentrations of TTC, OTC, and CTC was detected by using UV spectrophotometer (2600 UV/VIS, Unico Instrument Corporation, Shanghai) at 360 nm, 275 nm, and 370 nm, respectively. The concentrations of Cu and Mn were determined by using an atomic absorption-flame emission spectrometer (Thermo Scientific iCE3300, USA). A micro-electrophoresis meter (JS94F, Powereach, Shanghai) was employed to determine the zeta potential of samples. The data of the specific surface area were collected through the BET method by using surface area analyzer (V-Sorb X 800, Gold APP Instrument Corporation, Beijing). The crystalline structure was performed by means of X-ray diffraction technique (XRD-6100, Shimadzu Corporation, Japan). A field scanning electron microscope (S-3400N, Hitachi Limited, Japan) was employed to observe the morphology before and after reactions. The ultrastructure of sorbent was observed by transmission electron microscope (HT7700, Hitachi Limited, Japan). The thermal properties of sorbent were determined by means of thermogravimetric analysis (TGA-DSC 3+, Mettler Toledo, Switzerland). The data of the specific surface area was collected through the BET method by using surface area analyzer (V-Sorb X 800, Gold APP Instrument Corporation, Beijing). FTIR was employed to characteristic before and after reactions (Tensor 27, Bruker Optics, America). XPS data were collected by means of an X-ray photoelectron spectroscopy (AXIS ultra DLD, Shimadzu, Japan).

Results and discussion

Surface characteristics of MODCO

The powder X-ray diffraction pattern of MODCO is depicted in Fig. 1a. It can be seen that the material has obvious diffraction peaks, indicating a crystal structure. Through software

analysis and PDF standard card comparison, all diffraction peaks of MODCO can be indexed into four phases, including CuO (detected at $2\theta = 35.73°$, $38.89°$, $49.06°$, $66.12°$, $68.28°$, and $75.40°$), Cu_2O (at $36.57°$, $61.65°$, and $73.85°$), Mn_2O_3 (at $36.57°$, $61.65°$, and $73.85°$), and MnO_2 (at $23.83°$, $32.73°$, and $46.09°$). The grain sizes of $CuO \approx 0.76–0.41$ nm, $Cu_2O \approx 0.0.83–0.41$ nm, and $Mn_2O_3 \approx 0.0.83–0.41$ nm as well as $MnO_2 \approx 1.87–0.41$ nm were calculated based on the Scherrer equation, respectively.

For XPS analysis, the characteristic peaks of Cu2p, Mn2p, O1s, N1s, C1s, and Cl2p could be clearly inspected in the XPS all-scan spectrum shown as Fig. 1b, which demonstrated that Cu and Mn existed in the adsorbent. Meanwhile, the existence of a small amount of N and Cl could be attributed to the residual element in the preparation process of this adsorbent.

The N_2 adsorption-desorption isotherms of MODCO are shown in Fig. 1c, which seem to be typical type II isotherms according to the BDDT classification. The curve is biased to the vertical axis in the low pressure section and rises sharply at the high pressure end without adsorption saturation, indicating that the adsorbent is mostly mesoporous (Chen et al. 2014). The pore size distribution shown in Fig. 1d was mainly concentrated at 20–100 nm, which was consistent with the adsorption and desorption isotherms. Moreover, the surface area, pore size, and pore volume of MODCO was determined to be 67.74 m^2/g, 16.87 nm, and 0.286 cm^3/g, respectively. In

addition, the zeta potentials of MODCO at different pH conditions are measured and shown in Fig. 1e. The isoelectric point (IEP) of MODCO was about pH 7.82, indicating that the surface of this material is negatively charged at pH > 7.82 and positively charged at pH < 7.82. The thermogravimetry (TGA)-DSC result of MODCO is presented in Fig. 1f. The rapid weight loss of 12.2% in the first stage can be attributed to the evaporation of adsorbed water and bound water on the adsorbent surface when the temperature rises to 290 °C, while the light weight loss of about 3.8% in the second stage can be assigned to the loss of crystal water in the temperature range of 290–640 °C (Luengo et al. 2017). Additionally, the weight loss of 9.6% in the third stage is due to the dehydroxylation effect of Mn and Cu oxides from 640 to 870 °C (Panda and Kumar 2017). After that, the sample weight tends to be stabilized until T = 1000 °C.

The morphological structure of MODCO was obtained via the methods of SEM and TEM. Figure 2 shows the SEM images of copper oxide and MODCO, respectively. The morphology of copper oxide (shown in Fig. 2a) was formed by the aggregates of irregular spherical particles. The SEM image of MODCO in Fig. 2b shows needle-like structures of Mn oxides with sizes of 100–130 nm attached to the spherical Cu oxides with sizes of 50–100 nm, thereby forming a rough and compact surface. Figure S1 presents the results of EDS mapping analysis, indicating that the main elements of Cu, Mn, and O

Fig. 1 Surface characteristics of MODCO. **a** The XRD pattern of MODCO. **b** XPS spectrum and O1s spectrum of MODCO. **c** The nitrogen adsorption-desorption isotherms of MODCO. **d** The pore size distribution of MODCO. **e** Zeta potentials of MODCO at different pH conditions. **f** The TGA-DSC of MODCO
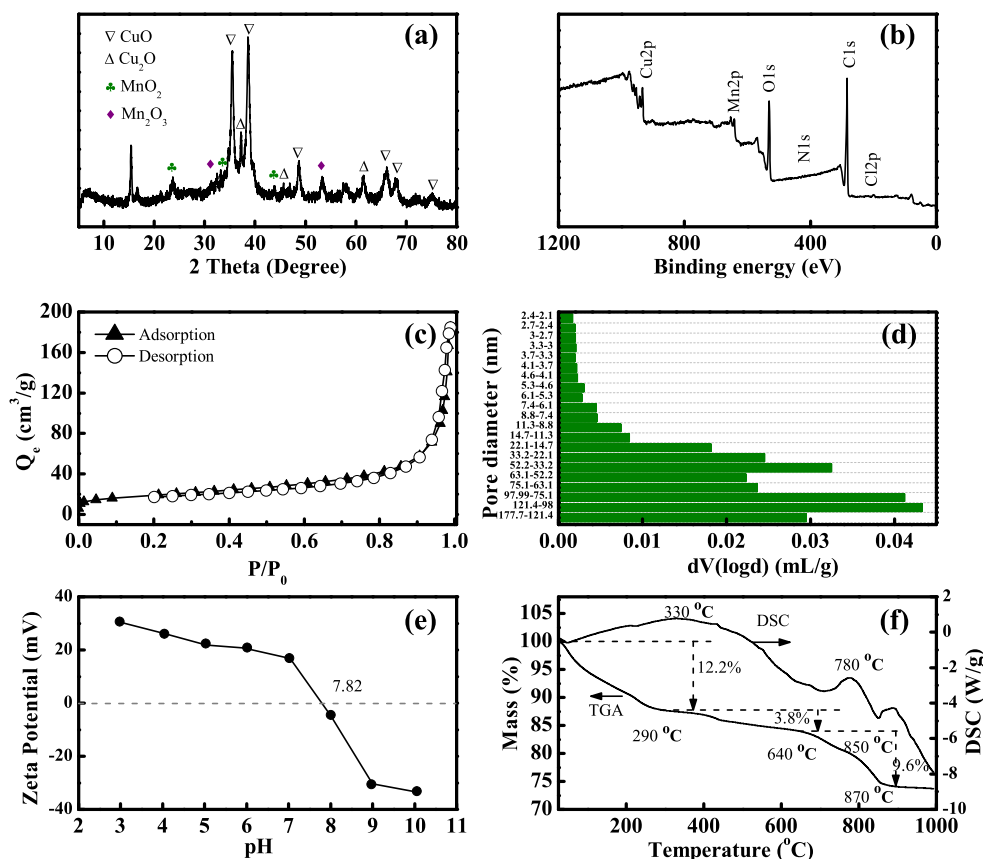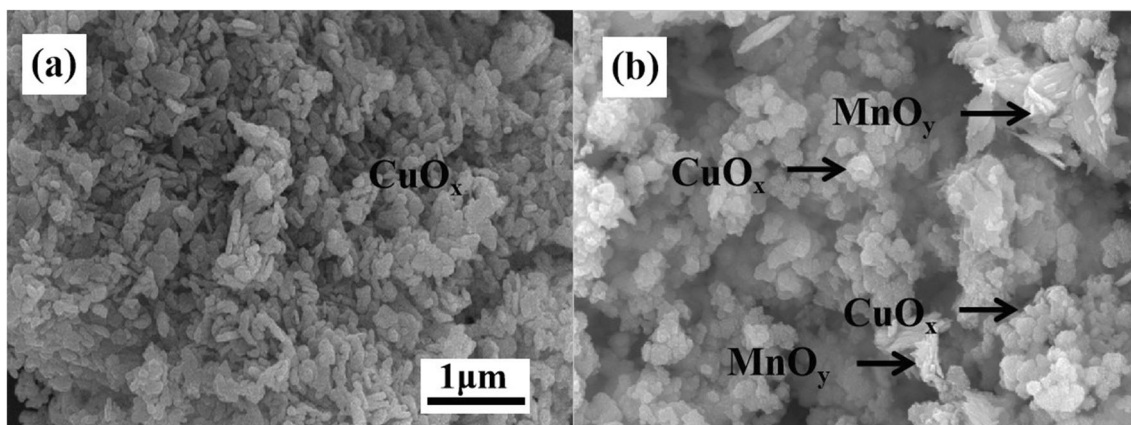
Fig. 2 SEM images of **a** copper oxide and **b** MODCO

within MODCO were evenly distributed on the composite surface. Moreover, the molar ratio of Cu/Mn on the material surface was about 2.74:1, which is very close to the designed value of 3:1. The TEM images of MODCO presented in Fig. S2 obtained at high resolution further confirm that the composite surface were formed via the aggregation of nanoscale particles of 20–100 nm with needle-like and irregular spherical structures.

Characteristic of TCs removal by MODCO

Sorption kinetics and equilibria

Figure 3 shows the kinetic curves for the removal of TTC, OTC, and CTC at different initial concentrations, namely 0.1 mmol/L and 0.5 mmol/L respectively. The removal amounts of TCs increased rapidly in the first 6 h, while the removal rate slowed down from 6 to 24 h. Afterwards, the removal processes gradually reached the equilibrium. Meanwhile, the removal amounts of TCs increased with the elevated concentrations of pollutants. The pseudo-second-order model, which described the kinetics of TCs satisfactorily, could provide more detailed information for comparing the removal rates of three TCs. Based on the k_2 values (shown in Table S2) for the removal of these TCs, their removal rates were in the order of OTC > CTC > TTC with the initial concentration of 0.1 mmol/L.

To evaluate the capability of MODCO for the removal of three TCs, the batch experiments were conducted at different initial concentrations. Figure 4 presents that the amounts of TCs removed by MODCO were elevated with the increased initial concentrations in the beginning and then became stable gradually. Finally, the removal amounts of all the three TCs reached a peak. Though the Langmuir isotherm equation is an empirical model, it was often used to evaluate the maximum removal capacity of materials by comparing the Langmuir q_m values. Hence, the maximum removal capacities of TTC,

OTC, and CTC were calculated as 2.901 mmol/g, 4.145 mmol/g, and 2.195 mmol/g according to the Langmuir model (Table S3), respectively. Table 1 demonstrates that the maximum removal capacities of MODCO for TCs are greater than that of some other adsorbents.
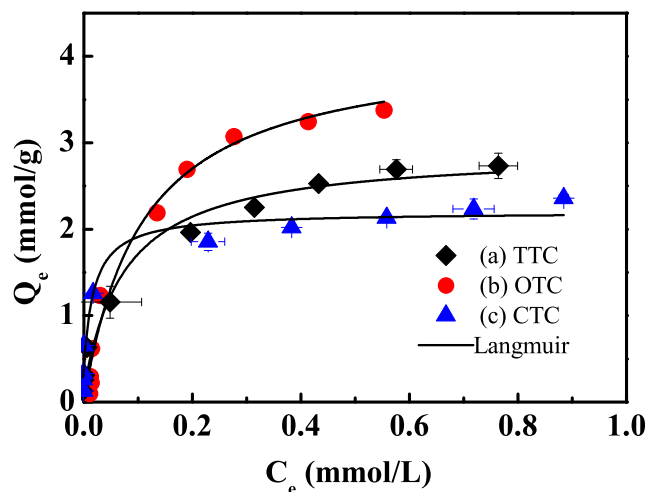
Effects of solution pH and coexisting ions

The pH value of aqueous solution is one of the most important water quality indexes that can affect removal performance. Hence, it is necessary to investigate the removal capacity of MODCO towards tetracycline antibiotics under different pH conditions. Figure S3 shows the distribution of tetracycline species with the change of solution pH. The predominant species of TTC is H_3L^+ at pH < 3.4, H_2L in the pH range of 3.4~7.6, and HL^- in the pH range of 7.6~9, as well as L^{2-} at pH > 9, respectively (Kang et al. 2011).The effects of pH on the removal of TTC, OTC, and CTC by MODCO were investigated and presented in Fig. 5a–c, respectively. A plateau for the removal amounts of TTC and CTC could be observed in the pH range of 7~9, while the better removal performance for OTC was obtained in the pH range of 6~8. It can be seen that when the pH was increased from 3 to 8, the removal amount of TTC increased gradually, and reached the peak (2.40 mmol/g) at pH 8. After that, the removal amount decreased remarkably with the further pH increase. The reduced removal efficiency of TTC at acidic (pH < 7) or alkaline (pH > 8) conditions could be explained by the electrostatic repulsion between MODCO and TTC species. Moreover, abundant hydroxyl ions could compete with the TTC species (mainly HL^- and L^{2-}) at pH > 8 for the active sites on MODCO, thereby intensifying the inhibitive effects of alkaline conditions. With the solution pH increases, the positive charge on the surface of the MODCO decreases, and the TTC is electrically neutral due to the loss of protons, the electrostatic repulsion decreased or even disappears consequently, and the adsorption effect gradually increases. As the pH rises further (> 8), the surface of
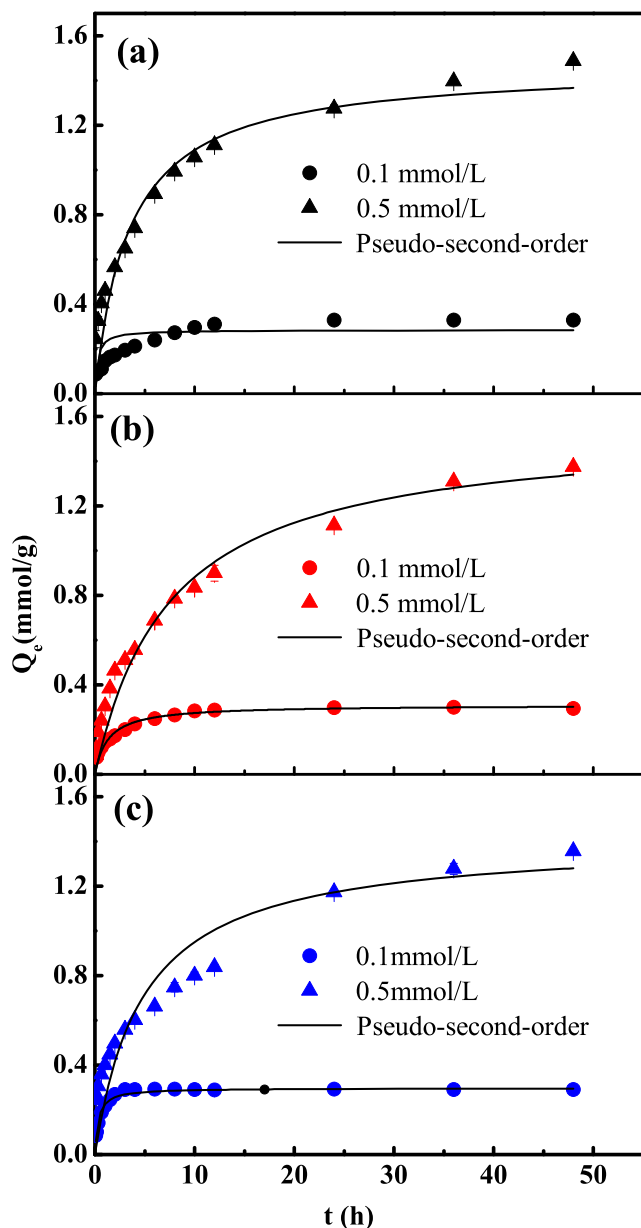
Fig. 3 Removal kinetics of TCs on MODCO. a TTC. b OTC. c CTC. Experimental conditions: initial concentrations = 0.1 or 0.5 mmol/L, adsorbent dosage = 0.3 g/L, pH = 7, ionic strength = 0.01-M NaNO₃, reaction time = 24 h

Fig. 4 Removal amounts of TCs by MODCO at different initial concentrations. a TTC. b OTC. c CTC. Experimental conditions: initial concentrations = 0.02~1.40 mmol/L, adsorbent dosage = 0.3 g/L, pH = 7, ionic strength = 0.01-M NaNO₃, reaction time = 24 h

MODCO is negatively charged, and TTC is also converted into the forms of anions HL^- and L^{2-} due to further loss of protons and the electrostatic repulsion between TTC and MODCO, resulting in the removal amount dropped. Overall, the optimum pH range for the removal of TTC and OTC is pH 6~9, while that for CTC removal is 7~9. Hence, excellent removal performances of TCs can be achieved by using MODCO without a pH adjustment of treated water. However, it is noted that the released Cu(II) concentrations from MODCO after the removal of TCs were increased at acidic or alkaline conditions. It means that there is a

requirement to optimize the chemical composition or the micro-structure of MODCO in future work.

To further evaluate the applicability of MODCO in actual TC-contaminated wastewater, the effect of common cations and anions on the removal of TCs was investigated and the results are presented in Fig. 6. It is shown that magnesium, phosphate, carbonate, and sulfate as well as nitrate ions had no significant influence on the removal of TTC and OTC. However, the presence of calcium and silicate ions depressed the removal of TTC and OTC, and the inhibition effect was intensified with increasing ions concentration, especially for calcium ion. The negative effects of calcium ion were mainly due to the complexation between TTC/OTC and calcium ion. The side effects of silicate ions were mainly attributed to the competition with TTC or OTC for the active sites on the surface of adsorbent. On the other hand, magnesium, calcium, phosphate, and sulfate as well as nitrate ions had no discernible effects on the removal of CTC. It is noted that the removal of CTC was barely affected by the coexistence of Ca^{2+} ions, though CTC can strongly form complex with bivalent cations. Some researchers found a similar result when they used magnetite nanoparticles for the adsorption of CTC. The adsorption of CTC was not inhibited unless the concentration of Ca^{2+} exceeded 10 mM (Zhang et al. 2011). Another difference between CTC and TTC and OTC is that carbonate and silicate ions showed slightly promotive effects on the removal of CTC, and the promotion effects became more pronounced with the increasing ion concentrations. The description of this phenomenon, which may be attributed to the different molecule structures and functional groups between TTC/OTC and CTC, depends on the further research on the interaction and competition mechanism between CTC and coexisting ions on the surface of MODCO.

**Table 1** Comparison of maximum TC adsorption capacities between MODCO and other adsorbents

Sorbent	Pollutant	Langmuir Q_m (mmol/g)	References
MODCO	TTC	2.901	Present study
MODCO	OTC	4.145	Present study
MODCO	CTC	2.195	Present study
Activated carbon	OTC	1.06	Alegakis et al. (2000)
Graphene	TTC	0.71	Gao et al. (2012)
Kaolinite	TTC	0.12	Zhao et al. (2011)
Clay	TTC	0.21	Chang et al. (2009)
Bamboo charcoal	TTC	0.11	Liao et al. (2013)
Activated sludge	OTC	0.18	Song et al. (2014)
Chitosan	TCs	0.934	Kang et al. (2010)

Removal mechanism

### Analysis of FTIR spectra

Figure 7 shows the FTIR spectra of MODCO samples before and after TCs removal. The bands at 3511 cm^{-1} and 3431 cm^{-1} were attributed to the stretching vibrations of hydroxyl groups (Liu et al. 2015).The peak at 1632 cm^{-1} could be ascribed to the deformation of water molecules, indicating the existence of adsorbed water on the material (Li et al. 2014). The peak at 1047 cm^{-1} might be corresponded to the

vibration of Cu-O (Pillewan et al. 2011). The remained absorption peaks below 800 cm^{-1} could be attributed to the stretching and bending vibrations of metal oxygen bonds (Liu et al. 2006). After the reaction with TTC, OTC, and CTC, several new characteristic peaks appeared at 1604 cm^{-1}, 1449 cm^{-1}, and 1328 cm^{-1}, as well as 1207 cm^{-1} could be assigned to the stretching vibration of C-H (Matsushima 1963), and the distortion vibration of CH$_2$ (Srinivasan et al. 2015) as well as the tensile deformation of C=O (Evangelin et al. 2012), respectively. This result confirmed that TC molecules have been successfully adsorbed onto the surface of MODCO. In addition, the bands for hydroxyl groups at 3511 cm^{-1}, 3431 cm^{-1}, 1632 cm^{-1}, and 1047 cm^{-1} showed a significant decrease in their intensity, indicating the involvement of hydroxyl groups in the removal of TCs. Furthermore, the peaks for nitrate (NO$_3^-$) at 858 cm^{-1} and 1376 cm^{-1} were weakened or even disappeared,
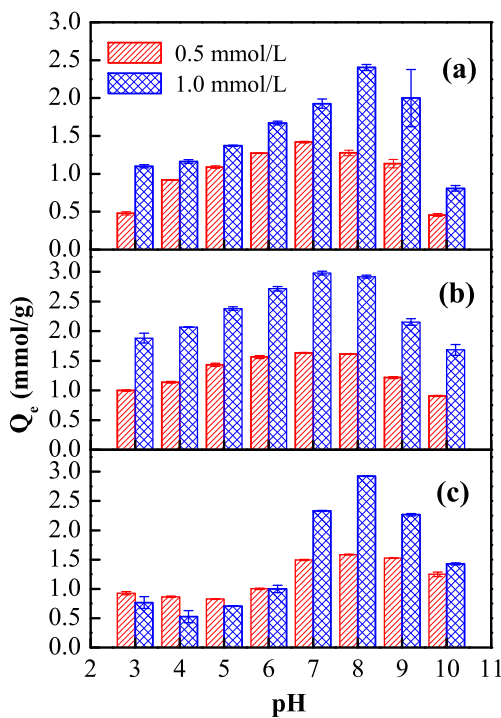
Fig. 5 The effect of solution pH on the removal of TCs by using MODCO. a TTC. b OTC. c CTC. Experimental conditions: initial concentration = 0.5 or 1.0 mmol/L, adsorbent dosage = 0.3 g/L, ionic strength = 0.01-M NaNO$_3$, reaction time = 24 h
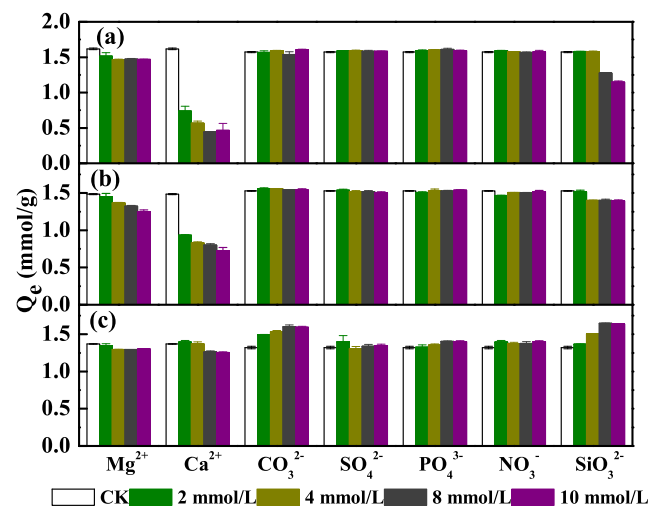
Fig. 6 The effect of coexisting ions on the removal of TCs by MODCO. a TTC. b OTC. c CTC. Experimental conditions: initial concentration = 0.5 mmol/L, adsorbent dosage = 0.3 g/L, pH = 7, ionic strength = 0.01-M NaNO$_3$, reaction time = 24 h
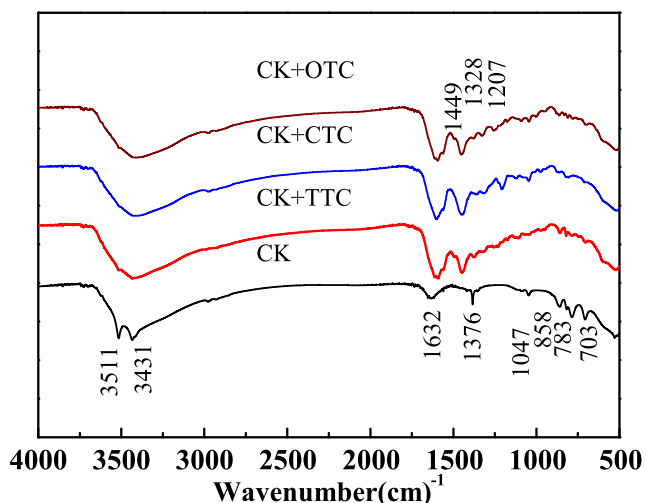
Fig. 7 The FTIR spectra of fresh MODCO and MODCO reacted with TCs

indicating that the impregnated nitrates were replaced by TCs via ion exchange process (Kavitha et al. 2012). Hence, we speculated that TCs can react with hydroxyl groups and other functional groups on the adsorbent surface, forming a surface complex at the water/adsorbent interface, and then be adsorbed on the surface of MODCO (Gu and Karthikeyan 2005).

Analysis of XPS spectra

To further investigate the removal mechanisms of TCs, Fig. S4 presents the wide-scan XPS spectra of MODCO before and after TC removal. After the reactions with TCs, the intensities of both C and N element peaks were increased after reactions, and the N element ratios were raised from 0.23 to 1.29%, 2.37%, and 1.46% after the removal of TTC, OTC, and CTC, respectively, thereby further confirming the removal of TCs onto MODCO. Moreover, Fig. 8 illustrates the O1s, Cu2p, and Mn2p spectra of the pristine and reacted samples. It can be seen from the O1s spectra (Fig. 8a) that the area ratios of Me-OH (531.5 eV) (Dedryvere et al. 2010) decreased from 42.78 to 33.75%, 22.55%, and 26.14% after the removal of TTC, OTC, and CTC, respectively, which corroborated the participation of hydroxyl groups in the removal of TCs. Meanwhile, the area ratios assigned to Me=O (529.7 eV) (Zhang et al. 2014) decreased from 7.32 to 5.92% and 2.81% as well as 5.88%, respectively. It was mainly explained by the reason that the Cu ions within MODCO can form complex Cu(II)-TCs with the combination of TCs and thus enhancing the removal of TCs (Tang et al. 2014; Zhang et al. 2015). In addition, two new oxygen peaks appeared at 533.5 and 531.5 eV, 533 and 531.3 eV, and 532.8 and 531.8 eV, respectively, which are characteristics of oxygen-
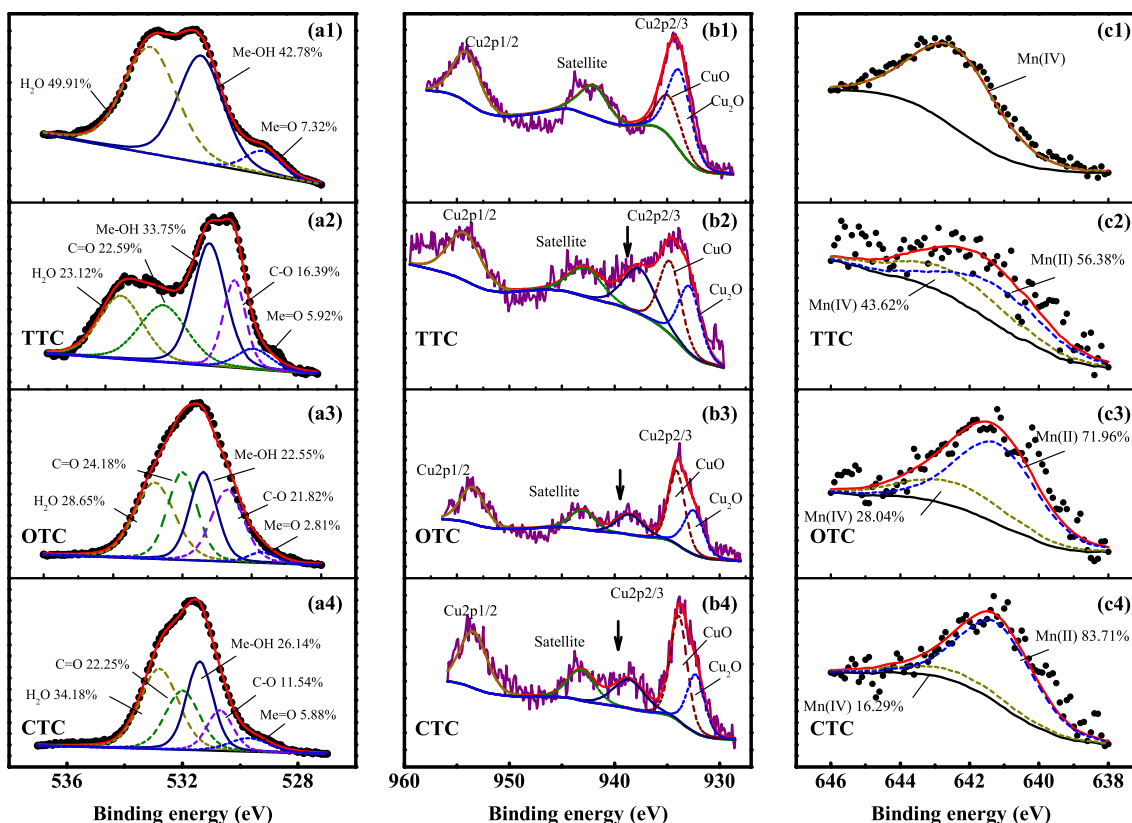
Fig. 8 The XPS spectra of MODCO before and after TCs sorption. **a** O1s. **b** Cu2p. **c** Mn2p

Fig. 9 The XPS spectra and UV spectrogram of MODCO after TC sorption. **a** C1s XPS spectra. **b** UV spectrogram
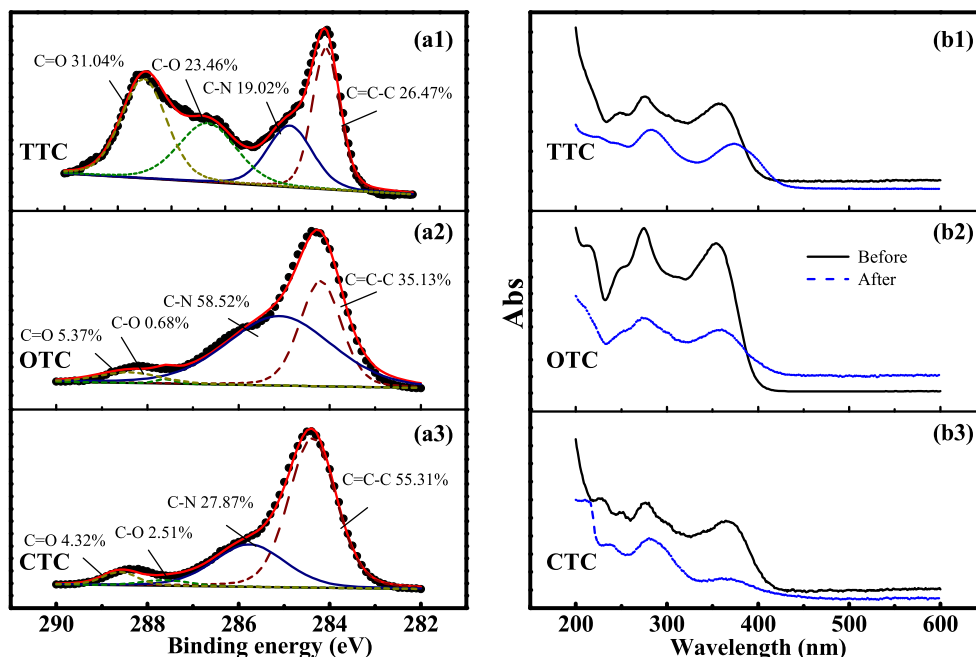
containing functional groups in TCs (C=O and C-O) (Lin et al. 2015).

The Cu valence state was analyzed by fitting $Cu2p_{1/2}$ (954.1 eV) and $Cu2p_{2/3}$ (934.2 eV) presented in Fig. 8(b1), while the satellite peaks at 934.8 eV and 933.8 eV were characteristic of $Cu2p_{2/3}$. The reactions with TTC, OTC, and CTC led to the formation of a new characteristic peak at 937.6, 938.5, and 938.6 eV, respectively (Fig. 8(b2–b4)), which were attributed to the combination of some oxygen-containing functional groups in TCs with released Cu(II) (shown in Fig. S5), thus indicating the affinity of Cu(II) for TCs (Zhang et al. 2015). As shown in Fig. 8(c1–c4), it can be seen obviously that a new peak corresponding to Mn(II) appeared at 641.2 eV in addition to the peak of Mn(IV) (642.4 eV) after the removal of TCs(Chen et al. 2014; Chen et al. 2018). In addition, the ratio of Mn(IV)/Mn(II) decreased from 1 to 0.77, 0.39, and 0.19 after the reaction with TTC, OTC, and CTC, respectively. This result indicated that MnO_2 may have a certain degree of oxidation effect on TCs during the removal process. As shown in Fig. S5, the release of Mn(II) from MODCO after TCs removal also indicated the dissolution of MnO_2 after the removal of TCs.

Figure 9 illustrates that the XPS C1s spectra and UV-visible absorption spectra of MODCO reacted with three kinds of TCs. As shown in Fig. 9a, the difference in fitting curves of C peak was ascribed to the different molecular structures of the three kinds of antibiotics, which was consistent with the results of FTIR analysis. It is further proved that TCs were successfully attached to the surface of MODCO. Moreover, it is also possible that TCs were partly oxidized by MnO_2 during the removal process resulting in different intermediates, because the previous studies have proved that

MnO_2 can play a key role in the adsorption and uncomplete composition of TTC and OTC (Dong et al. 2018; Rubert 2006). In addition, Fig. 9b shows the UV spectrograms of MODCO before and after the removal of TCs. There were certain changes at the peak position in the spectra after the reactions with the three antibiotics. The peaks at 360 nm were weaken or shifted after the removal of TCs, which suggested that there is a structural change in the p-electron system located on rings during the removal processes. Meanwhile, the intensity of the peak at 270 nm was decreased for OTC-reacted sample, indicating a damage of the tricarbonyl methane keto-enol system within OTC (Mahamallik et al. 2015). This UV-visible absorption results further confirmed that the redox processes involving MnO_2 are mainly responsible for the removal of TCs in a certain degree.

Conclusions

This work presents that MODCO is a promising adsorbent for the removal of three kinds of TCs from synthesized TC-contaminated water. The Mn oxides were evenly impregnated into the Cu oxides, and the optimal Cu/Mn molar ratio was 3:1 for TC removal. The plateau for the removal of TTC, OTC, and CTC could be achieved within 10 h, 10 h, and 3 h, respectively. On the other hand, the Langmuir Q_m values of TTC, OTC, and CTC were determined to be 2.90 mmol/g, 4.15 mmol/g, and 2.20 mmol/g, respectively. A favorable removal performance could be maintained in a wide pH range of 6~9, and there were unnoticeable inhibitive effects caused by the presence of common anions. The FTIR spectra results illustrated that the hydroxyl groups on adsorbent surface play

an important role in the removal of TCs. The XPS analysis results demonstrated that the removal mechanisms of TCs were mainly attributed to surface complexation. Furthermore, a certain oxidation effect of MODCO was proposed for the removal of TCs due to the oxidative activity of Mn oxides. Based on the above results, MODCO shows great potential to be used for the removal of TCs from aqueous solution. Unfortunately, the released Cu(II) ions at acidic or alkaline conditions may bring about a problem of second pollution. To solve this problem, MODCO needs to be further optimized in order to strengthen the stability of Cu component.

References

Alegakis AK, Tzatzarakis MN, Tsatsakis AM, Vlachonikolis IG, Liakou V (2000) In vitro study of oxytetracycline adsorption on activated charcoal. J Environ Sci Health B 35(5):559–569

Bangari RS, Sinha N (2019) Adsorption of tetracycline, ofloxacin and cephalexin antibiotics on boron nitride nanosheets from aqueous solution. J Mol Liq 293:111376

Belhouchet N, Hamdi B, Chenchouni H, Bessekhouad Y (2019) Photocatalytic degradation of tetracycline antibiotic using new calcite/titania nanocomposites. J Photochem Photobiol A Chem 372:196–205

Cao J, Xiong Z, Lai B (2018) Effect of initial pH on the tetracycline (TC) removal by zero-valent iron: adsorption, oxidation and reduction. Chem Eng J 343:492–499

Chang P, Li Z, Yu T, Munkhbayer S, Kuo T, Hung Y, Jean J, Lin K (2009) Sorptive removal of tetracycline from water by palygorskite. J Hazard Mater 165:148–155

Chen J, He F, Zhang H, Zhang X, Zhang G, Yuan G (2014) Novel core–shell structured Mn–Fe/$_{MnO2}$ magnetic nanoparticles for enhanced Pb(II) removal from aqueous solution. Ind Eng Chem Res 53: 18481–18488

Chen J, Wang J, Zhang G, Wu Q, Wang D (2018) Facile fabrication of nanostructured cerium-manganese binary oxide for enhanced arsenite removal from water. Chem Eng J 334:1518–1526

De Sousa DNR, Insa S, Mozeto AA, Petrovic M, Chaves TF, Fadini PS (2018) Equilibrium and kinetic studies of the adsorption of antibiotics from aqueous solutions onto powdered zeolites. Chemosphere 205:137–146

Dedryvere R, Foix D, Franger S, Patoux S, Daniel L, Gonbeau D (2010) Electrode/electrolyte interface reactivity in high-voltage spinel LiMn$_{1.6}$Ni$_{0.4}$O$_4$/Li$_4$Ti$_5$O$_{12}$ lithium-ion battery. J Phys Chem C 114:10999–11008

Dong G, Huang L, Wu X, Wang C, Liu Y, Liu G, Wang L, Liu X, Xia H (2018) Effect and mechanism analysis of MnO$_2$ on permeable reactive barrier (PRB) system for the removal of tetracycline. Chemosphere 193:702–710

Evangelin C, Naren S, Dharmendirakumar M (2012) Comparison of the surface features of the three chemically modified silk cotton hull activated carbons. Orient J Chem 28:1761–1768

Gao Y, Li Y, Zhang L, Huang H, Hu J, Shah SM, Su X (2012) Adsorption and removal of tetracycline antibiotics from aqueous solution by graphene oxide. J Colloid Interface Sci 368:540–546

Gao B, Chen W, Liu J, An J, Wang L, Zhu Y, Sillanpää M (2018) Continuous removal of tetracycline in a photocatalytic membrane reactor (PMR) with Zn$_{In2S4}$ as adsorption and photocatalytic coating layer on PVDF membrane. J Photochem Photobiol A Chem 364: 732–739

Grujić S, Vasiljević T, Laušević M (2009) Determination of multiple pharmaceutical classes in surface and ground waters by liquid chromatography–ion trap–tandem mass spectrometry. J Chromatogr A 1216:4989–5000

Gu C, Karthikeyan KG (2005) Interaction of tetracycline with aluminum and Iron hydrous oxides. Environ Sci Technol 39:2660–2667

Homem V, Santos L (2011) Degradation and removal methods of antibiotics from aqueous matrices–a review. J Environ Manag 92:2304–2347

Kang J, Liu H, Zheng Y, Qu J, Chen JP (2010) Systematic study of synergistic and antagonistic effects on adsorption of tetracycline and copper onto a chitosan. J Colloid Interface Sci 344:117–125

Kang J, Liu H, Zheng Y, Qu J, Chen JP (2011) Application of nuclear magnetic resonance spectroscopy, Fourier transform infrared spectroscopy, UV–visible spectroscopy and kinetic modeling for elucidation of adsorption chemistry in uptake of tetracycline by zeolite beta. J Colloid Interface Sci 354:261–267

Kavitha P, Jayaraj S, Raghav D (2012): Optical properties and density functional theory study of single crystal glycine. International Journal of Applied Physics and Mathematics, 293-295

Kim Y, Lee K, Choi K (2016) Effect of runoff discharge on the environmental levels of 13 veterinary antibiotics: a case study of Han River and Kyungahn Stream, South Korea. Mar Pollut Bull 107:347–354

Kushikawa RT, Silva MR, Angelo ACD, Teixeira MFS (2016) Construction of an electrochemical sensing platform based on platinum nanoparticles supported on carbon for tetracycline determination. Sensors Actuators B Chem 228:207–213

Li K, Yediler A, Yang M, Schulte-Hostede S, Wong MH (2008) Ozonation of oxytetracycline and toxicological assessment of its oxidation by-products. Chemosphere 72:473–478

Li G, Gao S, Zhang G, Zhang X (2014) Enhanced adsorption of phosphate from aqueous solution by nanostructured iron(III)–copper(II) binary oxides. Chem Eng J 235:124–131

Li J, Zhang H, Chen Y, Luo Y, Zhang H (2016) Sources identification of antibiotic pollution combining land use information and multivariate statistics. Environ Monit Assess 188:430

Liao P, Zhan Z, Dai J, Wu X, Zhang W, Wang K, Yuan S (2013) Adsorption of tetracycline and chloramphenicol in aqueous solutions by bamboo charcoal: a batch and fixed-bed column study. Chem Eng J 228:496–505

Lin HB, Huang WZ, Rong HB, Mai SW, Hu JN, Xing LD, Xu MQ, Li WS (2015) Improving cyclic stability and rate capability of LiNi$_{0.5}$Mn$_{1.5}$O$_4$ cathode via protective film and conductive polymer formed from thiophene. Solid State Electron 19:1123–1132

Liu Z, Ma R, Osada M, Iyi N, Ebina Y, Takada K, Sasaki T (2006) Synthesis, anion exchange, and delamination of Co–Al layered double hydroxide: assembly of the exfoliated nanosheet/polyanion composite films and magneto-optical studies. J Am Chem Soc 128: 4872–4880

Liu H, Yang Y, Kang J, Fan M, Qu J (2012) Removal of tetracycline from water by Fe-Mn binary oxide. J Environ Sci 24:242–247

Liu T, Wu K, Xue W, Ma C (2015) Characteristics and mechanisms of arsenate adsorption onto manganese oxide-doped aluminum oxide. Environ Prog Sustain Energy 34:1009–1018

Liu X, Huang D, Lai C, Zeng G, Qin L, Zhang C, Yi H, Li B, Deng R, Liu S, Zhang Y (2018a) Recent advances in sensors for tetracycline antibiotics and their applications. TrAC Trends Anal Chem 109: 260–274

Liu H, Yang Y, Sun H, Zhao L, Liu Y (2018b) Effect of tetracycline on microbial community structure associated with enhanced biological N&P removal in sequencing batch reactor. Bioresour Technol 256: 414–420

Liu H, Sun H, Zhang M, Liu Y (2019) Dynamics of microbial community and tetracycline resistance genes in biological nutrient removal process. J Environ Manag 238:84–91

Luengo CV, Volpe MA, Avena MJ (2017) High sorption of phosphate on Mg-Al layered double hydroxides: kinetics and equilibrium. J Environ Chem Eng 5:4656–4662

Ma J, Zhou B, Zhang H, Zhang W, Wang Z (2019) Activated municipal wasted sludge biochar supported by nanoscale Fe/Cu composites for tetracycline removal from water. Chem Eng Res Des 149:209–219

Mahamallik P, Saha S, Pal A (2015) Tetracycline degradation in aquatic environment by highly porous MnO_2 nanosheet assembly. Chem Eng J 276:155–165

Matsushima M (1963) The hydration of some organic compounds in an aqueous solution. I. Studies of aliphatic aldehydes by Raman-effect observation. B Chem Soc Jpn 36:954–960

Panda D, Kumar EA (2017) Surface modification of zeolite 4A molecular sieve by planetary ball milling. Mater Today Proceed 4:2

Pillewan P, Mukherjee S, Roychowdhury T, Das S, Bansiwal A, Rayalu S (2011) Removal of As(III) and As(V) from water by copper oxide incorporated mesoporous alumina. J Hazard Mater 186:367–375

Premarathna KSD, Rajapaksha AU, Adassoriya N, Sarkar B, Sirimuthu NMS, Cooray A, Ok YS, Vithanage M (2019) Clay-biochar composites for sorptive removal of tetracycline antibiotic in aqueous media. J Environ Manag 238:315–322

Rubert PJA (2006) Kinetics of oxytetracycline reaction with a hydrous manganese oxide. Environ Sci Technol 40:7216–7221

Saitoh T, Shibata K, Hiraide M (2014) Rapid removal and photodegradation of tetracycline in water by surfactant-assisted coagulation–sedimentation method. J Environ Chem Eng 2:1852–1858

Selmi T, Sanchez-Sanchez A, Gadonneix P, Jagiello J, Seffen M, Sammouda H, Celzard A, Fierro V (2018) Tetracycline removal with activated carbons produced by hydrothermal carbonisation of Agave americana fibres and mimosa tannin. Ind Crop Prod 115: 146–157

Song X, Liu D, Zhang G, Frigon M, Meng X, Li K (2014) Adsorption mechanisms and the effect of oxytetracycline on activated sludge. Bioresour Technol 151:428–431

Srinivasan G, Suresh G, Sumalatha M (2015) Synthesis, growth and characterization of organic nonlinear optical crystal of glycine sodium acetate (GSA) for optical applications. Mater Today: Proc 2: 4592–4599

Tang W, Zeng G, Gong J, Liang J, Xu P, Zhang C, Huang B (2014) Impact of humic/fulvic acid on the removal of heavy metals from aqueous solutions using nanomaterials: a review. Sci Total Environ 468-469:1014–1027

Wang Z, Chen Q, Zhang J, Dong J, Yan H, Chen C, Feng R (2019a) Characterization and source identification of tetracycline antibiotics in the drinking water sources of the lower Yangtze River. J Environ Manag 244:13–22

Wang W, Han Q, Zhu Z, Zhang L, Zhong S, Liu B (2019b) Enhanced photocatalytic degradation performance of organic contaminants by heterojunction photocatalyst $BiVO4/TiO2$/RGO and its compatibility on four different tetracycline antibiotics. Adv Powder Technol 30: 1882–1896

Watkinson AJ, Murby EJ, Kolpin DW, Costanzo SD (2009) The occurrence of antibiotics in an urban watershed: from wastewater to drinking water. Sci Total Environ 407:2711–2723

Xu Z, Fan J, Zheng S, Ma F, Yin D (2009) On the adsorption of tetracycline by calcined magnesium-aluminum hydrotalcites. J Environ Qual 38:1302–1310

Xu Z, Song X, Li Y, Li G, Luo W (2019) Removal of antibiotics by sequencing-batch membrane bioreactor for swine wastewater treatment. Sci Total Environ 684:23–30

Yan C, Yang Y, Zhou J, Liu M, Nie M, Shi H, Gu L (2013) Antibiotics in the surface water of the Yangtze Estuary: occurrence, distribution and risk assessment. Environ Pollut 175:22–29

Zhang D, Niu H, Zhang X, Meng Z, Cai Y (2011) Strong adsorption of chlorotetracycline on magnetite nanoparticles. J Hazard Mater 192: 1088–1093

Zhang G, Ren Z, Zhang X, Chen J (2013) Nanostructured iron(III)-copper(II) binary oxide: a novel adsorbent for enhanced arsenic removal from aqueous solutions. Water Res 47:4022–4031

Zhang LL, Ma YL, Cheng XQ, Zuo PJ, Cui YZ, Guan T, Du CY, Gao YZ, Yin GP (2014) Enhancement of high voltage cycling performance and thermal stability of $LiNi_{1/3}Co_{1/3}Mn_{1/3}O_2$ cathode by use of boron-based additives. Solid State Ionics 263:146–151

Zhang Z, Liu H, Wu L, Lan H, Qu J (2015) Preparation of amino-Fe(III) functionalized mesoporous silica for synergistic adsorption of tetracycline and copper. Chemosphere 138:625–632

Zhao Y, Geng J, Wang X, Gu X, Gao S (2011) Tetracycline adsorption on kaolinite: pH, metal cations and humic acid effects. Ecotoxicology 20:1141–1147

Zhou L, Ying G, Liu S, Zhang R, Lai H, Chen Z, Pan C (2013) Excretion masses and environmental occurrence of antibiotics in typical swine and dairy cattle farms in China. Sci Total Environ 444:183–195